Deep–Sea Research I 217 (2025) 104455



Contents lists available at ScienceDirect

Deep-Sea Research Part I

journal homepage: www.elsevier.com/locate/dsri

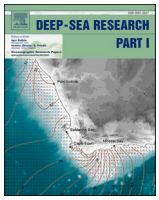

Strong magnetism and geochemical characteristics of sediment in Challenger Deep and their indications for sources

KaiWei Wang [a], YongHong Wang [a,b,*], QiuYu Yue [a], XiaoHua Zhang [c], JiWen Liu [c], Chunhui Xiao [a], Toshiya Kanamatsu [d,e], Michael Strasser [f], Rui Bao [g]

[a] Key Lab of Submarine Geosciences and Prospecting Techniques, MOE and College of Marine Geosciences, Ocean University of China, Qingdao, 266100, China
[b] Laboratory for Marine Geology, Qingdao Marine Science and Technology Center, Qingdao, 266237, China
[c] Frontiers Science Center for Deep Ocean Multispheres and Earth System, and College of Marine Life Sciences, Ocean University of China, Qingdao 266003, China
[d] Research Institute for Marine Geodynamics, JAMSTEC, Marine Geology and Geophysics Research Group, Subduction Dynamics Research Center Kanagawa, 237-0061, Japan
[e] Japan Agency for Marine-Earth Science and Technology (JAMSTEC), Research Institute of Marine Geodynamics (IMG) Yokosuka, 237-0061, Japan
[f] University of Innsbruck, Institute of Geology Innsbruck, Austria
[g] Frontiers Science Center for Deep Ocean Multispheres and Earth System, And Key Laboratory of Marine Chemistry Theory and Technology, Ministry of Education, Ocean University of China Qingdao, 266100, China

ARTICLE INFO

Keywords:
Challenger deep
Sediment provenance
Sediment activation

ABSTRACT

Understanding the properties of trench sediments is an important aspect of comprehending the sources and transport variations of trench sediments. This study seeks to identify the sources of sediment and understand the mechanisms driving sediment source variation in the Challenger Deep, based on the environmental magnetic characteristics and geochemical properties of the MT20-750 core retrieved from a depth of 10,815 m in the Mariana Trench. The proximal sediment source of the MT20-750 core comprises mainly altered bedrock components from the southern Pacific Plate and volcanic eruption materials from the northern Philippine Plate, while the distal source is primarily aeolian dust input, with biogenic materials also contributing. The overall magnetic susceptibility values of the sediments in the Challenger Deep are significantly higher, reaching 3–5 times that of other regions in the Pacific Ocean. The strong magnetic properties of these sediments are primarily due to the enhanced alteration of the southern subducting plate rocks, which are mainly composed of basalt rich in iron and magnesium (mafic basalt), under the action of Pacific bottom water. This represents a normal state when sediments are funneled into the trench axis and preserved in an oxidizing environment. However, the sediments from the northern Philippine Sea Plate, mainly composed of tuffaceous rocks with lower Fe, Mg, and Ti content, intermittently enter the trench during seismic events or turbidity flows. These events alter the sediment composition in the trench, leading to a decrease in magnetic susceptibility values, with the change in provenance primarily driven by the varying intensity of geological processes and the specific conditions of sediment transport.

1. Introduction

Trench science represents the forefront of contemporary oceanographic research, with the unique morphology and depth of trenches posing significant challenges for studying sediment sources and deposition patterns. For example, the Mariana Trench is a product of the subduction of the Pacific Plate beneath the Philippine Sea Plate, characterized as a non-accretionary margin (Zhang et al., 2014). The Challenger Deep, located in the southwestern part of the Mariana Trench, is recognized as the deepest point on Earth (Fig. 1), with recent bathymetric studies indicating a maximum depth of 10,924 ± 15 m (Bongiovanni et al., 2022). The northern slope on the landward side is 3.0° between 5000 and 8000 m and 8.9° below 8000 m. On the seaward side, the southern slope is 1.7° between 5000 and 8000 m and 10.2° below 8000 m (Fig. 1c). The abyss features a unique asymmetrical "V"-shaped profile, which facilitates the accumulation and storage of

* Corresponding author. Key Lab of Submarine Geosciences and Prospecting Techniques, MOE and College of Marine Geosciences, Ocean University of China, Qingdao, 266100, China
E-mail address: yonghongw@ouc.edu.cn (Y. Wang).

https://doi.org/10.1016/j.dsr.2025.104455
Received 18 September 2024; Received in revised form 29 December 2024; Accepted 24 January 2025
Available online 25 January 2025
0967-0637/© 2025 Elsevier Ltd. All rights are reserved, including those for text and data mining, AI training, and similar technologies.

sediments along the trench axis (Jamieson, 2015; Turnewitsch et al., 2014). The extreme depth and narrow geomorphology of the Challenger Deep result in high hydrostatic pressure and hydrological isolation, creating a unique sedimentary system and significantly complicating sampling efforts. Consequently, the Challenger Deep remains one of the least studied regions on Earth.

Previous research on the Mariana Trench has largely focused on its formation (Larson et al., 1975; Bloomer, 1983, 1987; Stern et al., 2003), the rheological structure and dynamics of the lithosphere (Gao et al., 2017), and the hydrodynamic characteristics of deep and bottom waters (Taira et al., 2004). These studies have primarily addressed the tectonic conditions responsible for deformation in the Parece Vela Basin and Mariana Trench, as well as the dynamics of deep and bottom waters at the Challenger Deep. In contrast, more recent studies have increasingly turned to sediment analysis, seeking to improve our understanding of sedimentary stratigraphy, chronology, depositional processes and environments, and the sources of sediments within the trench. For example, Deng et al. (2016) conducted the first magnetostratigraphic study on the sediment core JL7KGC01A from the southern Mariana Trench, providing valuable insights into sedimentary processes and the influence of Antarctic Bottom Water (AABW) in the region. Their work also laid the foundation for a preliminary stratigraphic sequence and chronological framework for the core. In a similar vein, Luo et al. (2017) examined the redox conditions during the Last Glacial Maximum (LGM) by analyzing major, trace, and rare earth elements in cores from the southern Mariana Trench, shedding light on past environmental conditions. Furthermore, several studies have focused on the identification of sediment sources through the rare earth element geochemistry of sediments from the southern Mariana Trench (Wang et al., 2016; Jiang et al., 2019). Jiang et al. (2019) notably identified significant contributions from Asian dust in a sediment core retrieved from a depth of 5525 m. Furthermore, Song et al. (2022) proposed that the primary sources of Challenger Deep sediments are a combination of marine materials, largely derived from volcanic activity on Luzon Island, and terrestrial materials, especially Asian dust. This conclusion was based on the analysis of four sediment cores collected from depths ranging from 5800 to 10,954 m. Similarly, Xie et al. (2024) classified the sediments of the Challenger Deep into four main types: red-brown deep-sea clays, siliceous biogenic mud, secondary sediments, and calcareous biogenic mud. These sediment types are primarily governed by three key factors: bedrock weathering, bioclastic deposition, and early diagenesis.

Although potential sediment sources for the Challenger Deep have been identified, there remains a need for more rigorous quantification of these sources and a comprehensive understanding of the sedimentary processes occurring in deep-sea trenches. In response to this gap, the present study aims to quantitatively analyze the sediment sources and develop a model of sedimentary processes through environmental magnetic measurements, grain size analysis, geochemical testing, and SEM observations on approximately 7 m of core sediments from the Challenger Deep (Fig. 1). This research provides valuable insights into sediment dynamics in deep-sea trench environments with limited terrigenous input. Furthermore, the findings contribute to refining sediment transport models, thus advancing sedimentological theories at both regional and global scales.

Fig. 1. (a) Locations of sediment cores analyzed in this study, including MT20-750 (red stars). Additional sample locations (red dots) are from MD06-3047 (Xu et al., 2015), D149-D152 (Chen et al., 2020), and F100901-F101012 (Meng et al., 2006). The yellow line represents the Antarctic Bottom Water (AABW) boundary. (b) Locations of samples BC-11, CD-1, and GC-5 (Jiang et al., 2019), as well as sample L3 (unpublished data) (red dots), overlaid on a bathymetric contour map of the area outlined in red in panel (a), with contour intervals of 1000 m. (c) AB profile from panel (b), with data sourced from the National Oceanic and Atmospheric Administration.

2. Materials and methods

2.1. Geological setting and core sampling

The Mariana Trench is a result of the subduction of the Pacific Plate (the underlying plate) beneath the Philippine Sea Plate (the overlying plate), forming a non-accretionary margin. The Philippine Sea Plate is predominantly composed of tuffaceous rocks, while the Pacific oceanic crust, found in the forearc of the South Mariana Trench, consists of harzburgite, olivine gabbro, gabbro, diabase, and basaltic pillow lava (Reagan et al., 2013). The Mariana Trench-Island Arc-Trough system is characterized by a high central and low lateral free-air gravity anomaly (Gao et al., 2017). At a depth of 10,890 m, the maximum current speed was 8.1 cm/s, primarily driven by tidal, inertial, and long-period currents. Westward flow dominated at both northern and southern stations, with no cyclonic circulation observed at 142°35′E in the trench (Taira et al., 2004).

The core, MT20-750, was collected in 2020 using a gravity corer in the Challenger Deep in the Mariana Trench (11°19.904′N, 142°12.083′E) (Fig. 1). The water depth at the sampling site was 10,815 m, and the column length was 749 cm. The researchers subsampled the upper section (0–178 cm) at 1–3 cm intervals and the lower section (178–749 cm) at 25–53 cm intervals, resulting in 81 samples. The uppermost 225 cm of the MT20-750 sediment core consisted predominantly of dark brown silt, and the sediment properties of 225–749 cm generally show a brownish clayed silt composition.

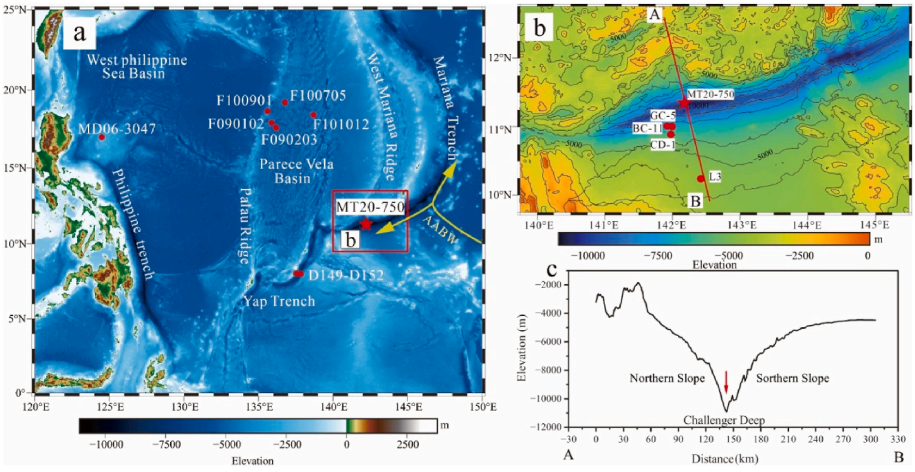

Fig. 1. Regional map and sample locations in the Marianas Trench area.

2.2. Particle size analysis and endmembers

Prior to particle size analysis, the samples were subjected to a series of pretreatments to eliminate the interference of biogenic calcite, biogenic silica and organic matter. For each of the 81 samples, approximately 0.3 g of sediment was placed in a 15 ml centrifuge tube and sequentially treated with ultra-pure water, 15% H_2O_2 solution, 20% glacial acetic acid solution and 2.0 mol/L Na_2CO_3 solution to remove sea salt, organic matter, carbonate and biogenic silica components from the sediments. Subsequently, 5 ml of sodium hexametaphosphate (0.05 mol/L) was added to disperse the samples before analysis to prevent flocculation.

Particle size analysis was conducted using a Mastersizer-2000 (UK) laser particle size analyzer with a 1/4 Φ particle size spacing and a relative error of less than 2% for repeated measurements. Particle size parameters were calculated using the moments method (McManus, 1988). The particle size measurements of all samples were performed at Key Lab of Submarine Geosciences and Prospecting Techniques, China.

Grain endmember analysis (EM) refers to a particle size data processing method that separates different sediment dynamics grain-level components from multi-source, multi-dynamic assemblages of sediments, which helps to more deeply interpret sediment provenances, dynamical conditions, and the paleoclimate and paleoenvironmental evolution information (Su et al., 2023; Wang et al., 2022). The Analysis program was run in the Matlab environment, and the Gen. Weibull parameterization method (Paterson and Heslop, 2015) was selected to perform a grain size endmember analysis of the MT20-750 core sediments. Considering linear correlation, angular deviation, and end-element correlation, three endmembers were finally selected for the analysis of MT20-750 core data.

2.3. Magnetic measurements

(1) The low frequency (0.47 kHZ) and high frequency (4.7 kHZ) magnetic susceptibilities of the samples were measured using a Bartington-MS2 magnetic susceptibility system, and then the frequency magnetization $\chi_{fd}=(\chi_{lf} - \chi_{hf})/\chi_{lf} \times 100\%$ was calculated.

(2) Application of 2G-760 superconducting magnetometer to obtain anhysteretic Remanent magnetization (ARM) at 100 mT AC field, 0.05 mT DC field.

(3) The isothermal remanent magnetization at an external field of 1 T field strength (considered as saturated isothermal remanent magnetization (SIRM)) was obtained using a 2G Enterprise pulsed magnetometer, after which the samples were sequentially magnetized in the inverse fields of 20 mT, 100 mT, and 300 mT to obtain IRM-20mT, IRM-100mT, and IRM-300mT, respectively, and the relevant magnetic parameters were calculated as follows (Evans and Heller, 2003; Thompson and Oldfield, 1986).

$$S_{-ratio} = -IRM_{-300mT}/SIRM \quad (1)$$

$$S_{-100} = 100 \times (SIRM - IRM_{-100mT}) / (2 \times SIRM)(\%) \quad (2)$$

$$S_{-300} = 100 \times (SIRM - IRM_{-300mT}) / (2 \times SIRM)(\%) \quad (3)$$

(4) The hysteresis loops (LOOP), IRM acquisition curves, and reverse field demagnetization curves of two representative samples were measured on a vibrating sample magnetometer (VSM8600) (maximum field setting of 1T, step size of 5 mT) to obtain saturation magnetization (Ms), saturation remanence (Mrs), coercivity (Hc) and coercivity of remanence (Hcr).

The magnetic susceptibility measurements in the environmental magnetic measurements were performed at the Key Lab of Submarine Geosciences and Prospecting Techniques, and the rest of the tests were done at the Key Laboratory of Paleomagnetism and Tectonic Reconstruction, Ministry of Natural Resources.

2.4. Scanning electron microscope

Six samples from MT20-750 cores were selected for SEM (JSM-7610F) analysis at 12 cm, 76 cm, 93 cm, 111 cm, 137 cm, and 225 cm layers by Marine Equipment Inspection &Testing, Qingdao. The magnetic particles were extracted by low intensity magnetic separation method before SEM observation. Other non-magnetic particles were also "entrained" during the extraction of magnetic particles. Finally, high resolution SEM was used to analyze the type, shape, and microstructure of the magnetic minerals.

2.5. Geochemical analysis and Sc-Th-Zr/10 ternary diagram analysis

A total of 53 samples at suitable intervals were reselected to analyze major and trace elements using X-ray fluorescence spectrometer (XRF) and inductively coupled plasma mass spectrometry (ICP-MS).

Major elements analysis (XRF): The samples were dried and ground to less than 200 mesh; the samples were accurately weighed using a one-tenth of a millionth of a balance and mixed with lithium tetraborate. (0.5000g of sample, 1.5000g of lithium tetraborate); Place the mixed sample in a washed platinum crucible and make fuse piece; After the piece is cooled, mark the sample and use X-ray fluorescence spectrometer (ZSX Primus II) to determine the content of the major elements (i.e., Si, Al, Fe, K, Na, Ca, Mg and Ti), and the content of each component in the sample was calculated by converting the burned loss of the sample.

Trace elements analysis (ICP-MS): The sample was ground to 200 mesh in an agate mortar, dried at 110 °C for 3h, and transferred to a sealed desiccator. After cooling, weighed 40.00 mg of the sample accurately in a polytetrafluoroethylene liner, added 1.50 ml of high-purity HNO_3 and 1.50 ml of high-purity HF was distilled by sub boiling and shaken well. Put the liner into the stainless steel sleeve, tighten the sleeve cover, and put it into the drying oven, keep it at 190 °C for more than 48h, take out the liner after cooling, put it on the electric heating plate and steam it to wet salt phase, then add 1 ml of sub boiling distilled HNO_3 and steam it dry (to remove the residual HF), then add 3 ml of 1:1 nitric acid solution prepared by sub boiling distilled high purity HNO_3, keep it at 150 °C for 24h to ensure complete extraction of the sample. After cooling, the extraction solution was transferred to a clean PET bottle and fixed to 80.00 g with 2% dilute HNO_3 to be measured.

The trace elements in the samples were determined using a Varian 820 inductively coupled plasma mass spectrometry. The measured elements relative standard deviations (RSDs) were less than 5%, which met the requirements.

δCe Calculation: The δCe calculation is given by: $\delta Ce=(Ce/La)_{sample}/(Ce/La)_{PASS}$, where $(Ce/La)s_{ample}$ is the ratio of cerium (Ce) to lanthanum (La) in the sample, and $(Ce/La)_{PAAS}$ is the ratio of Ce to La in the Post-Archean Average Shale (PAAS), which serves as the standard for Earth's crust composition.

Sc-Th-Zr/10 Ternary Diagram: The Sc-Th-Zr/10 ternary diagram can be used to indicate sediment sources, as there are distinct differences in the distribution of volcanic materials, fresh bedrock, and various types of altered bedrock in the ternary diagram (Xie et al., 2024).

2.6. Discriminant function

Discriminant function (DF) analysis can describe the relationship between sediments and their possible provenance areas semi-quantitatively. The specific equation is as follows:

$$DF = (C_{1x} / C_{2x}) / (C_{1L} / C_{2L}) - 1$$

Where (C_{1x}/C_{2x}) represents the ratio of the two elements in the sediments of the study area, and (C_{1L}/C_{2L}) represents the ratio of the two

elements in the possible provenance area. Absolute values of DF less than 0.5 indicate that the two are more similar, and the smaller the absolute value of DF, the greater the correlation they have (Jiang et al., 2019; Wang et al., 2016; Xiao et al., 2020b; Xu et al., 2008). To reflect the degree of similarity more effectively, the heavy rare earth element ratio Lu/Yb was selected for discriminant function analysis of volcanic materials near the study area. The light rare earth elements ratio Sm/Nd was used for discriminant function analysis of erosional losses, which are relatively more stable during sediment transport and deposition.

3. Result

3.1. Sediment characteristics and age model

The MT20-750 sediment core is predominantly composed of dark brown to brownish silt. Based on the ^{14}C dating of bulk organic carbon from this core, the overall age ranges from approximately 3700 to 6000 years BP, with certain layers showing age reversals (Liu et al., 2024) (Fig. 2).

Based on the stable age range of 5150 to 4395 years BP and a sediment thickness of 106 cm (with no age reversals) for the 384–490 cm layer (Liu et al., 2024), the sedimentation rate is calculated to be 140.4 cm/kyr. For the 40–111 cm layer, which has a stable age range of 3765–4295 years BP and a sediment thickness of 71 cm (no age reversals), the sedimentation rate is 134.0 cm/kyr (Fig. 2). Therefore, over the past 6000 years, the average sedimentation rate in the Challenger Deep is estimated to be approximately 137 cm/kyr, assuming no age reversals.

3.2. Particle size

Based on grain size characteristics, combined with sampling intervals, magnetic and chemical features, the MT20-750 sediment core is divided into two major sections: A (0–225 cm) and B (225–749 cm). Section A is further subdivided into A0 (0–28 cm), A1 (28–100 cm), A2 (100–123 cm), and A3 (123–225 cm) (Fig. 2, Table 1). Due to data limitations, Section B is currently classified as a single section.

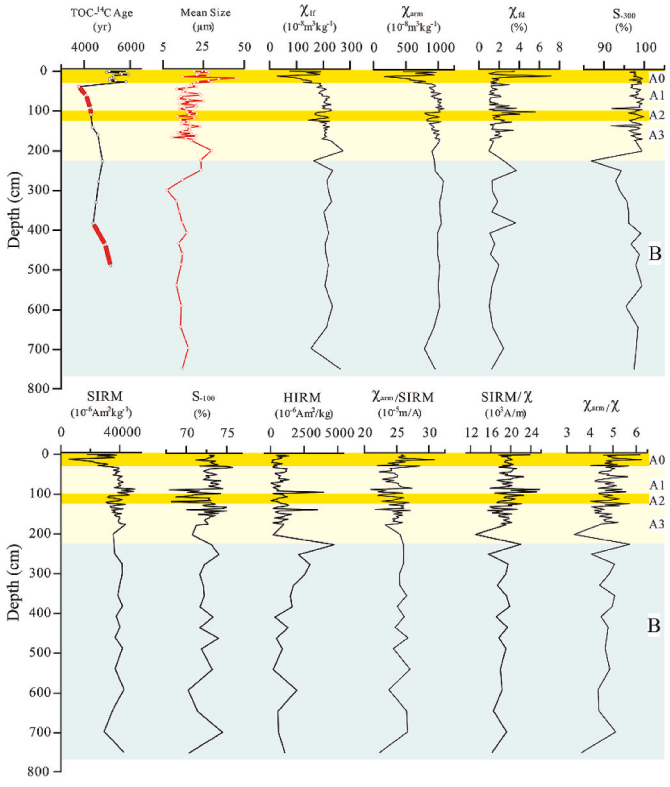

Fig. 2. Grain size parameters, environmental magnetic characteristics and TOC-^{14}C age with depth of core MT20-750. Here, TOC-^{14}C ages are cited from Liu et al. (2024).

According to Shepard (1954) grain size classification method, most sediment samples from the MT20-750 core are sandy silt, with a smaller portion being silty sand and clayey silt (Fig. 3). The overall range of mean grain size in the MT20-750 core samples is 7.0–45.6 μm, with an average of 20.2 μm. The grain size characteristics of each section are shown in Table 1. The sediments in Section B have the smallest grain size, with an average of only 15.0 μm, which is generally smaller than those in Section A. Section A0 has the largest overall grain size, with an average of 28.2 μm; the mean grain size of sections A1, A2, and A3 is relatively stable, showing a gradual decrease with increasing depth (Fig. 2).

3.3. Environmental magnetic characteristics

Environmental magnetism links the magnetic properties of mineral mixtures to the environmental processes (Liu et al., 2012). The type, concentration and grain size of the magnetic minerals affect environmental magnetic properties. Provenance, diagenesis and autogenous mineral are some environmental factors that control these characteristics (Thompson and Oldfield, 1986; Evans and Heller, 2003; Xiao et al., 2020a).

3.3.1. Types of magnetic minerals

SIRM/χ is often used as a preliminary indicator to differentiate the types of magnetic minerals in the sample (Peters and Dekkers, 2003; Roberts, 1995). The values of SIRM/χ for each segment of MT20-750 are relatively low and vary little, with a range of 13.0–25.7 $\times$ 10^3 Am^{-1}. Conversely, the values of χ for the sample are relatively high and exhibit a range of 26.9–274.0 $\times$ $10^{-8}m^3kg^{-1}$ (Fig. 2; Table 1). This suggests that the magnetic minerals in the sample are dominated by ferrimagnetic minerals (Peters and Dekkers, 2003).

The corrected magnetic hysteresis parameters of the MT20-750 sample also support this result. As shown in Fig. 5ab, after a 70% paramagnetic correction, the hysteresis loop for the sample in the MT20-750 completely closes between 200 and 300 mT, presenting a high and narrow shape. This suggests that the coercivity of the magnetic mineral is within this range, indicating that the primary magnetic mineral in the sample is magnetite. Under the SEM, various forms of magnetite were observed in different layers, including octahedrons, rhombic dodecahedrons, and aggregates (Fig. 4). The single-crystal magnetite structure was intact. The size of individual magnetite crystals was typically less than 1 μm, and the magnetite in the sample was mostly in the form of aggregates.

The S_{-Ratio} can be used to detect the relative abundance of low coercivity ferrimagnetic minerals and high coercivity antiferromagnetic minerals (such as hematite and goethite) (Liu et al., 2012; Thompson and Oldfield, 1986). When the S_{-300} value is greater than 90% or close to 1, it indicates that low coercivity ferrimagnetic minerals dominate. As the content of high coercivity magnetic minerals in the sample increases, the S-Ratio gradually decreases and eventually approaches 0 (King and Channell, 1991; Wang et al., 2017). As shown in the table, the S_{-300} values of the MT20-750 samples are consistently high, with most values exceeding 95%, indicating that the magnetic minerals in the samples are primarily low-coercivity ferromagnetic minerals (e.g., magnetite). Specifically, the S_{-300} values in Section A are overall stable (>97%), while the S_{-300} values in Section B (<97%) are lower than those in Section A, suggesting the input of other weakly magnetic minerals. Meanwhile, the HIRM value of the core increases in section B (Fig. 2), indicating that the proportion of the hard component (e.g., hematite) began to increase in this section.

Table 1
Mean values of magnetic parameters of sediments in each section of core MT20-750.

Sections	Mean size (μm)	χ_{lf} ($10^{-8}m^3kg^{-1}$)	χ_{arm} ($10^{-8}m^3kg^{-1}$)	χ_{fd}%	SIRM ($10^{-6}Am^2kg^{-1}$)	S_{300}	HIRM ($10^{-6}Am^2kg^{-1}$)	χ_{arm}/χ	χ_{arm}/SIRM ($10^{-5}mA^{-1}$)	SIRM/χ (10^3Am^{-1})
A0	28.2	131.5	656.1	2.5	25522.9	97.9	541.4	5.1	26.0	19.6
A1	19.0	203.6	972.4	1.6	40002.4	98.1	789.9	4.8	24.4	19.7
A2	19.4	184.7	892.7	2.6	36424.5	97.9	719.2	4.9	24.7	19.8
A3	19.4	210.1	958.3	1.8	38341.2	97.1	1114.8	4.6	25.1	18.4
B	15.3	216.2	993.2	1.8	38963.8	96.7	1311.0	4.6	25.6	18.1

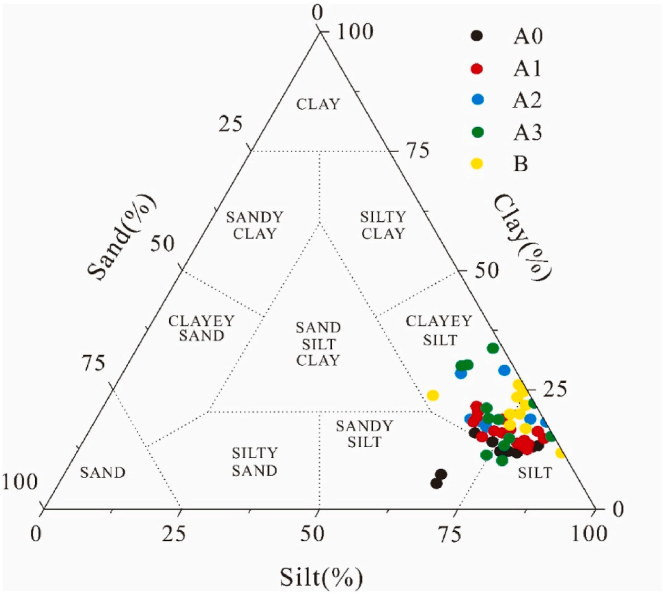

Fig. 3. Shepard classification of sediment grain size in each section of core MT20-750.

3.3.2. Magnetic mineral content

The χ parameter is commonly used as an indicator of the concentration of paramagnetic minerals in sediment samples. However, as χ is affected by multiple factors, χ_{ARM} and SIRM are often selected in conjunction with χ to indicate the content of magnetic minerals in the sample (Maher, 1988; Thompson and Oldfield, 1986). The values of χ, χ_{ARM}, and SIRM in the MT20-750 core are higher compared to other sediment samples, indicating a higher content of magnetic minerals. The magnetic mineral content in Section B is higher than in Section A (Table 1). Most layers in Section A have slightly higher magnetic susceptibility (average 216 × 10^{-8} m^3/kg) compared to Section B (average 206 × 10^{-8} m^3/kg), but A0 (average 131 × 10^{-8} m^3/kg) and A2 (average 184 × 10^{-8} m^3/kg) are lower, being only 60% and 85% of Section B, respectively (Fig. 2). The χ_{ARM} and SIRM parameters show similar trends to χ. In samples from A2, many diatoms were observed (Fig. 4c–e), a phenomenon not found in other sections. Previous sediment cores from the Mariana Trench have also reported diatom mats (Luo et al., 2018; Zhang et al., 2021), consistent with the characteristics of this section. The dilution effect of diatoms in the sediments may be the reason for the reduced magnetism in Section A2.

3.3.3. Magnetic mineral particle size

The χ_{ARM}/χ and χ_{ARM}/SIRM ratios are widely used as indicators of the ferrimagnetic mineral particle size (Banerjee et al., 1981; Liu et al., 2012; Peters and Dekkers, 2003). The χ_{ARM}/χ and χ_{ARM}/SIRM ratios of the MT20-750 core are relatively stable, with low values ranging from 4.4 to 5.1 and 24.4–26.0 mA^{-1} respectively, indicating the absence of single-domain (SD) particles of bacterial origin in the samples (Yamazaki, 2009) and mainly composed of pseudo-single-domain (PSD) particles (0.1–1 μm). Furthermore, the King diagrams can be used for semi-quantitative discrimination of magnetic mineral particle size in samples (King et al., 1982). In the King diagram (Fig. 5c), the magnetic mineral particles in the sediment of core MT20-750 are mainly distributed in the range of 0.1μm–1μm, corresponding to PSD particles, with a small portion of SD particles that have a particle size close to 0.1 μm.

3.4. Geochemical characteristics and rare earth element source discrimination

3.4.1. Geochemical characteristics

The characteristics of major elements, rare earth elements, and redox-sensitive elements in the MT20-750 sediment core are shown in Fig. 6. The Al_2O_3 content in the core remains stable in Section B, but begins to increase from Section A3 upwards, with a particularly notable surge in Section A2. The average Al_2O_3 content in Section A2 reaches 18.1%, approximately 5% higher than in other sections. The contents of TiO_2, Fe_2O_3, and MgO exhibit a high degree of consistency in their variations: they remain stable in Section B and then show a general decreasing trend upwards.

In recent years, significant enrichment of rare earth elements (REEs) has been discovered in deep-sea sediments in various regions of the Pacific Ocean (Kashiwabara et al., 2018; Kato et al., 2011). In contrast, the total REE content in the MT20-750 sediment core is relatively low, with an average of 121.9 μg/g, and shows a decreasing trend from the bottom to the top. The redox environment of sediments can be assessed using δCe as an indicator, with negative Ce anomalies typically indicating an oxic to suboxic environment (Luo et al., 2018).

Based on the REE histogram of MT20-750 (Fig. 6), it is inferred that the entire MT20-750 core was deposited in an oxic to suboxic environment, with no anoxic layers detected.

3.4.2. Sediment source discriminant function (DF) characteristics

Rare earth elements are excellent geochemical tracers and have been used in some studies to explore the sources, sedimentary environments, and sedimentary processes of sediments in the Philippine Sea and the Mariana Trench regions (Jiang et al., 2019; Luo et al., 2017; Xiao et al., 2020b; Xu et al., 2008).

The discriminant function of Table 2 indicates that the DF values of the MT20-750 core are less than 0.5, suggesting that all sources in the table contributed to the sample. For instance, the DF values for the related samples from the nearby Mariana Trench volcanic material are significantly lower than 0.15, indicating their substantial contribution. Numerically, the MT20-750 core samples show the closest relationship with the West Mariana Ridge with a DF value of 0.02, followed by the Kyushu-Palau Ridge with a DF value of 0.08. The DF values for the basalt of the Mariana Trough and Parece Vela Basin are 0.12 and 0.13, respectively, while the DF value for the Chinese loess is the highest at 0.4. As a result, the sample has a relatively smaller contribution to the source compared to the nearby sources, which is consistent with environmental magnetic analysis results.

3.4.3. Sc-Th-Zr/10 ternary diagram for source discrimination

The Sc-Th-Zr/10 ternary diagram provides indications of sediment sources (Fig. 7). Volcanic materials, fresh bedrock, and different types of altered bedrock can be distinctly differentiated in the diagram. In this

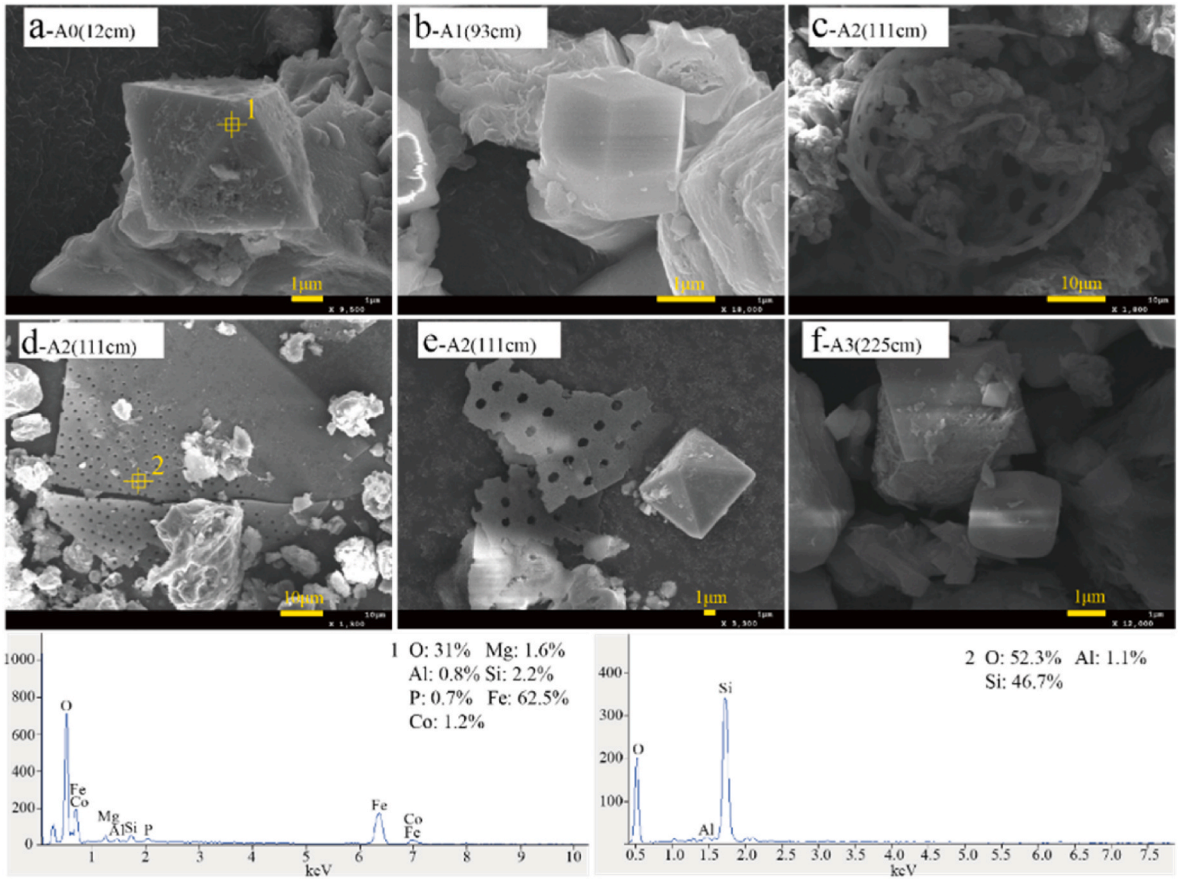

Fig. 4. SEM images and EDX results of some layers of MT20-750. (a) taken from section A0 (12 cm), octahedral magnetite crystals; (b) taken from section A1 (93 cm), rhombic dodecahedral magnetite crystals; (c) taken from section A2 (111 cm), radiolarian crushed shell; (c, d and e) taken from section A2, which contain diatom fragments; (f) taken from section A3 (137 cm) with 225 cm, magnetite fragments.

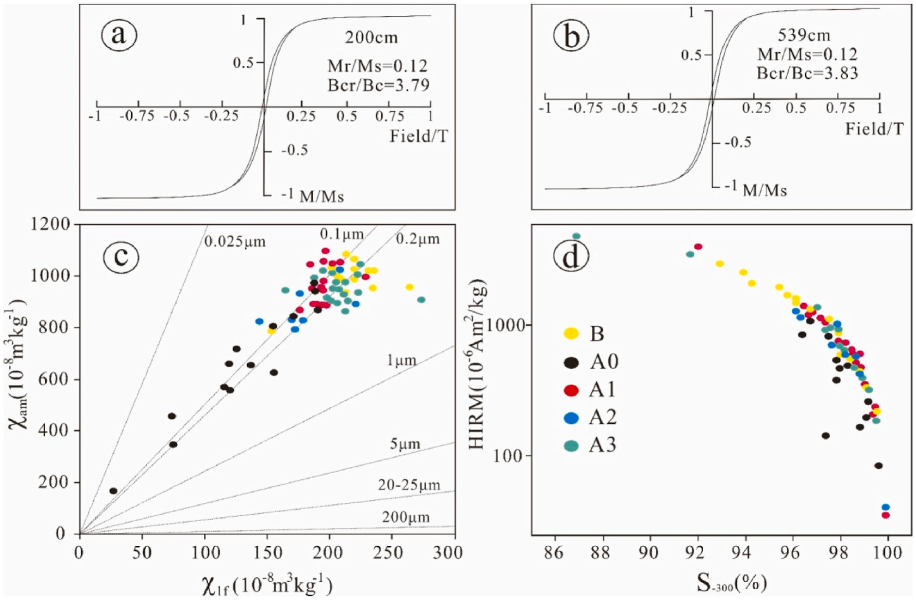

Fig. 5. Environmental magnetism characteristics of magnetic minerals in core MT20-750. (a and b) Hysteresis echoes of samples at depths of 200 cm and 539 cm; (c) King plot; (d) S_{-300}-HIRM scatter plot.

study, the sediment samples fall within the regions representing various types of altered bedrock, particularly zeolite facies altered bedrock and partially altered bedrock. This further suggests that the sediments in the Mariana Trench's Challenger Deep include detritus derived from nearby altered bedrock, consistent with previous studies in the area (Xie et al., 2024).

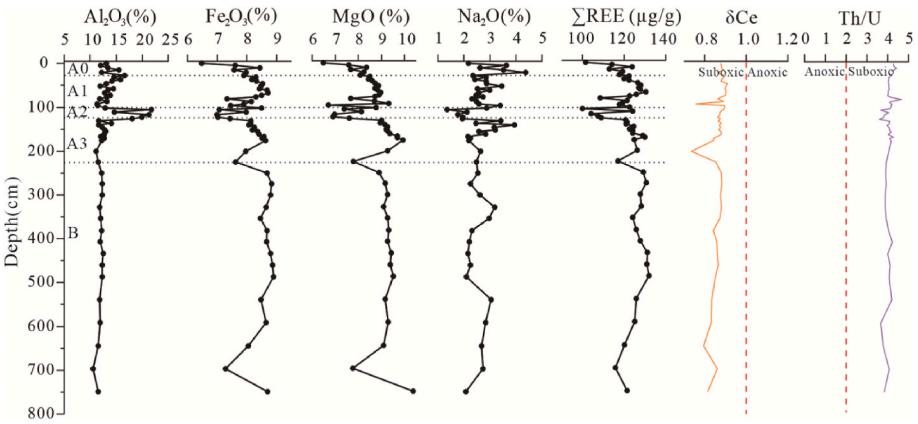

Fig. 6. Characteristics of some major and trace elements in the MT20-750 core.

Table 2
Discrimination function (DF) for samples of MT20-750 core sediments and sediments around the Marianas Trench.

Sample	Volcanic sources				Terrigenous sources
	Tuff from Kyushu-Palau Ridge	Tuff from West Mariana Ridge	Tuff from Parece Vela Basin	Basalt from Mariana Trough	Chinese loess
MT20-750	0.08	0.02	0.13	0.12	0.40
C-P19	0.09	0.03	0.12	0.11	0.37
L3	0.08	0.02	0.14	0.12	0.44
Sinking particles in Mariana Trench	0.09	0.05	0.13	0.12	0.35
Deep-sea clay in East Philippine Sea	0.07	0.02	0.12	nd	0.33

Note: Lu/Yb and Sm/Nd data used in the calculations of Tuff from Kyushu-Palau Ridge, West Mariana Ridge, Parece Vela Basin (Migdisov et al., 1981), basalt from Mariana Trough (Tian et al., 2003), Chinese loess (Wen et al., 1996), C-P19 and L3(Xiao et al., 2021), Mariana trench (Xiao et al., 2020b), Deep sea clay in East Philipping Sea (Xu et al., 2008).

3.5. Grain size endmember analysis

A grain size endmember analysis was conducted on the MT20-750 core data, with the results shown in Fig. 8. The analysis revealed that the sediment from the three endmembers of the MT20-750 core had characteristic grain sizes of EM1 (5 μm), EM2 (24 μm), and EM3 (70 μm), respectively. EM1 was identified as the predominant endmember, accounting for around 35%–50% of the sample, while EM2 accounted for around 30%–45%, and EM3 ranged from around 5%–35%. Previous research on sediment from the Philippine Sea indicates that the grain size of sediment components derived from Asian dust is typically less than 16 μm (Chen et al., 2020; Zhou et al., 2015). Furthermore, Xie et al. (2019) study revealed that aeolian dust particles within the core retrieved from the Western Pacific predominantly ranged in size from 1.51 to 4.26 μm. Thus the grain size of EM1 (5 μm) in this study corresponds well with this characteristic, suggesting the presence of Asian dust components. The major components of sediment in the region also include local altered bedrock, which may be transported by the Antarctic Bottom Water (AABW). The component from altered bedrock is the particle size of EM2. Similarly, Song et al. (2022) reported an

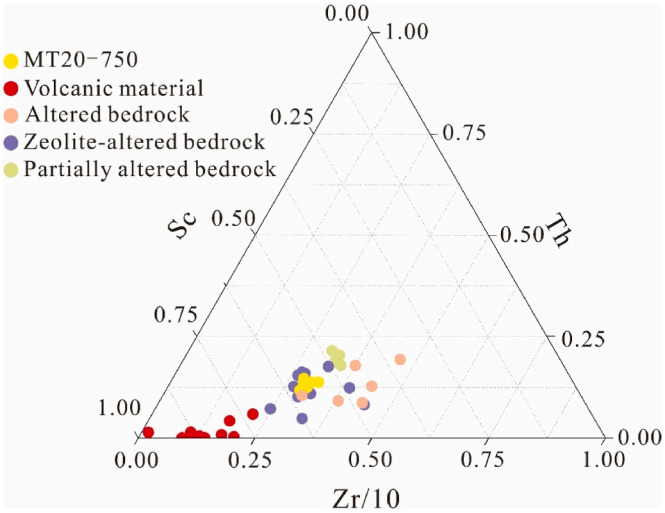

Fig. 7. Sc-Th-Zr/10 Ternary Diagram of Sediments of MT20-750 (this study), volcanic material (Wood et al., 1981), nearby altered bedrock, Zeolite altered bedrock, and Partially altered bedrock (Xie et al., 2024) in the Mariana Trench's Challenger Deep.

average particle size of 21.40 μm within the core retrieved from the Pacific Plate, which is similar to the particle size of EM2 (24 μm) in this study.

The grain size characteristics of EM3 were comparable to the main grain size endmembers from the C-P19 core in the northern part of the study area (75 and 81 μm, 162 μm, and 177 μm) and biogenic biogenic materials with larger size. Therefore, the grain size of EM3 (70 μm) in this study corresponds well with this characteristic, suggesting the input of the Philippine Sea Plate volcanic materials. Therefore, we conclude that the three endmembers identified in the sediment of the MT20-750 core represent the following: EM1–Asian dust and other fine-grained sediments (35–50%); EM2–sediment components from the southern Challenger Deep (30–45%); and EM3–sediment components from the northern Challenger Deep and biogenic materials (5–35%).

4. Discussion

4.1. Sediment provenance in Challenger Deep

Previous studies have demonstrated that Asia, following Africa, stands as the second largest contributor to global wind-blown dust emissions. This significantly adds to the particulate matter in vast oceans such as the Pacific, notably transporting an estimated 70 million tons of

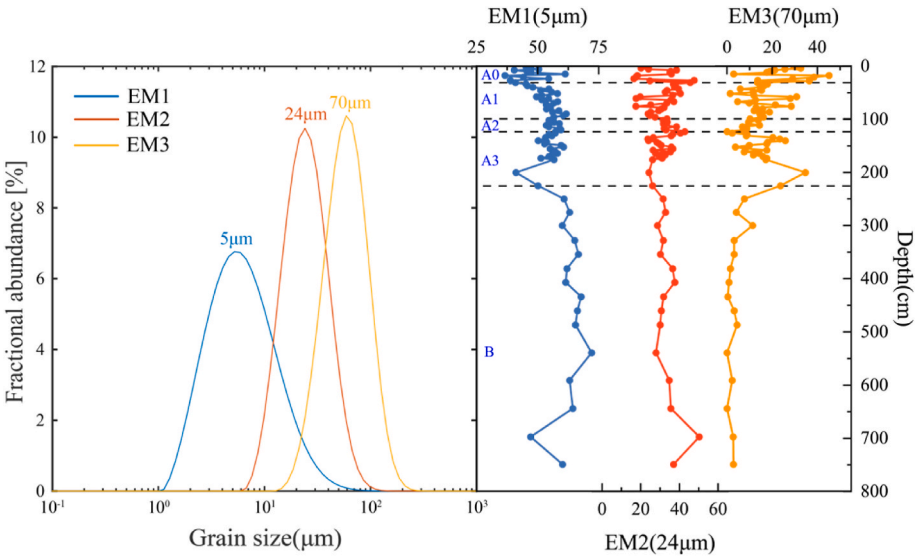

Fig. 8. Comprehensive diagram of grain size endmember of sediments in core MT20-750.

dust annually to the northwest Pacific (Shao et al., 2011). Recent investigations by Wang (2020) have refined this contribution to a precise range of 42%–44%, based on a two-end-member mixing model of rare earth elements. This firmly confirms the substantial influence of Asian continental dust on sediments in the region surrounding the Mariana Trench.

Jiang et al. (2019) determined that approximately 28% of the sediment in a core, retrieved from a depth of 5525 m on the southern slope of the Mariana Trench, comprised aeolian dust, employing the two-endmember mixing model. Subsequently, Song et al. (2022) uncovered that the proportion of aeolian dust in cores extending below 5800 m on the southern slope could attain up to 50%, utilizing Sr-Nd isotope analysis. The present study, utilizing the ternary grain size end-member analysis, quantitatively validates the substantial input of aeolian materials, with the EM1 component accounting for approximately 30–50% of the sediment, further confirming the significant contribution of aeolian material. In summary, considering both the proximity to the continent and the sedimentation rate of approximately 137 cm/kyr (around 1.3 mm per year, Fig. 2), the Challenger Deep, located beneath the East Asian monsoon region, likely has a high flux of aeolian dust deposition. This indicates that the sediments within this area probably contain a significant proportion of aeolian dust.

In addition to the substantial contribution from aeolian dust, other sediment sources in the Challenger Deep have also been documented. These include primarily volcanic origins from the Philippine Sea Plate (Jiang et al., 2019; Luo et al., 2018; Song et al., 2022; Wang et al., 2016), material derived from the alteration of subducting plate rocks and overlying plate bedrock (Xie et al., 2024), as well as biogenic material (Luo et al., 2018).

4.2. *High magnetic characteristics of sediments in the Challenger Deep*

As shown in Fig. 9, the χ and SIRM values reveal a notably higher content of magnetic minerals in the sediments of the Challenger Deep compared to other environments. These sediments display exceptionally elevated magnetic susceptibility, ranging from 26.9 to 274.0 $\times 10^{-8}$ m^3/kg (an average of 194.0 $\times 10^{-8}$ m^3/kg). This is markedly higher, approximately 3–5 times, than the susceptibility observed in other regions (Fig. 9). For comparison, the magnetic susceptibility of sediments from the Japan Trench ranges from 72.5 to 204.2 $\times 10^{-8}$ m^3/kg, with an average of 104.5 $\times 10^{-8}$ m^3/kg (Strasser et al., 2024). Similarly, the average magnetic susceptibility of sediments from the East China Sea Inner Shelf is 53.6 $\times 10^{-8}$ m^3/kg (Ma, 2011), and that from the Yellow River and Yangtze River is approximately 92.7 $\times 10^{-8}$ m^3/kg (Wang et al., 2004) (Fig. 9a), which fall significantly below the values in the Challenger Deep. Furthermore, the magnetic susceptibility of sediments from the Atlantic Basin, which spans from 5 to 70 $\times 10^{-8}$ m^3/kg, is substantially lower than that observed in our study area. Similarly, studies of sediments in other regions, such as the East Philippine Sea and the Pacific Ocean, reveal lower magnetic susceptibility values. In the East Philippine Sea, the range is 4.6–23.1 $\times 10^{-8}$ m^3/kg, while in the Pacific Ocean, it spans from 27.6 to 84.7 $\times 10^{-8}$ m^3/kg. Both of these

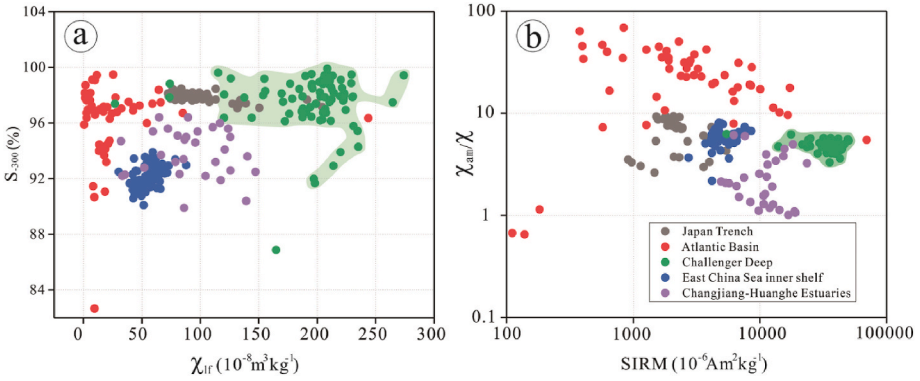

Fig. 9. Comparison of magnetic parameters in different sedimentary environments.

ranges are significantly lower than the values observed in the Challenger Deep region (Meng et al., 2007; Xiao et al., 2020a).

Especially, the magnetic susceptibility of sediments in northern area of the Challenger Deep is observed to be slightly lower (Fig. 10a). For instance, the sediment samples collected from Sites F090102-F101012 and C-P19, located in the northern section, exhibit magnetic susceptibility values within the ranges of 5.1–19.0 $\times 10^{-8}$ m^3kg^{-1} and 27 to 84 $\times 10^{-8}$ m^3kg^{-1}, respectively (Meng et al., 2006; Xiao et al., 2020a). In contrast, sediments collected from Sites L3 and D152, positioned in the southern area, demonstrate notably higher magnetic susceptibility, ranging from 200 to 265 $\times 10^{-8}m^3kg^{-1}$ and 278 to 385 $\times 10^{-8}m^3kg^{-1}$, respectively. (Xiao et al., 2020b; Chen et al., 2020) (Fig. 10a).

As shown in Fig. 9, the S_{-300} values imply a higher content of ferromagnetic minerals, such as magnetite (Fig. 9b). Furthermore, the χ_{ARM}/χ ratios suggest that the magnetic particles within the samples are predominantly pseudo-single domain (PSD) particles, ranging from 0.1 to 1 μm. These particles are notably coarser than those typically found in other sedimentary environments and do not encompass bacterial single domain (SD) particles. Consequently, the strong magnetic properties of the sediments can be primarily attributed to the higher content of coarse magnetite particles.

The data of sample category Japan Trench are cited from (Strasser et al., 2024), sample Atlantic Basin (Tang, 2021); data of sample East China Sea inner shelf (Ma, 2011); sample Changjiang-Huanghe Estuaries (Wang et al., 2004).

4.3. *Reasons for strong magnetic properties of sediments in the Challenger Deep*

Notably, the magnetic susceptibility values of this study surpass those of the northern regions but close to the southern regions adjacent to the Challenger Deep, while may infer that the sediments in the Challenger Deep are mainly caused by the sources from the southern regions. It is worth mentioning that the northern side of the Challenger Deep lies within the Philippine Sea Plate, which is largely composed of tuffaceous rocks characterized by lower Fe, Mg, and Ti content (Migdisov et al., 1981) (Fig. 10c). These tuffaceous rocks are associated with extensive volcanic tuff deposits found in the Kyushu-Palau Ridge, Mariana Trough, West Mariana Ridge, and Parece Vela Basin on the northern side of the Challenger Deep (Migdisov et al., 1981) (Fig. 1a). Topographically, the northern part of the Challenger Deep is adjacent to a series of high-relief island arcs. Under these circumstances, sediments originating from the overlying plate on the north side of the trench tend to accumulate on the northwest side of the island arcs, making it less likely for them to cross over and limiting sediment transport from the northern area.

However, the southern side of the Challenger Deep is primarily composed of Pacific oceanic crust rocks from the forearc of the South Mariana Trench, which encompass harzburgite, olivine gabbro, gabbro, diabase, and basaltic pillow lava (Reagan et al., 2013). These rocks are characterized by higher Fe, Mg, and Ti content (Fig. 10c) (Xie et al., 2024). Furthermore, Fig. 10c reveals strong magnetic anomalies in the Pacific Plate of the Mariana Trench (Hu et al., 2014), which enhance the magnetic properties of the altered rock debris in this region. Additionally, the modern bottom water in the Mariana Trench is rich in oxygen (Luo et al., 2018), and the δCe values indicate an oxic to suboxic depositional environment (Fig. 6). This environment does not favor early diagenetic reduction processes that would dissolve magnetite in the original samples, thus having little effect on the magnetic mineral content in the sediment core. Consequently, the magnetic properties of the sediments in the Challenger Deep are primarily attributed to the Pacific Plate, and the favorable oxidation conditions help preserve the strong magnetism of the sediments.

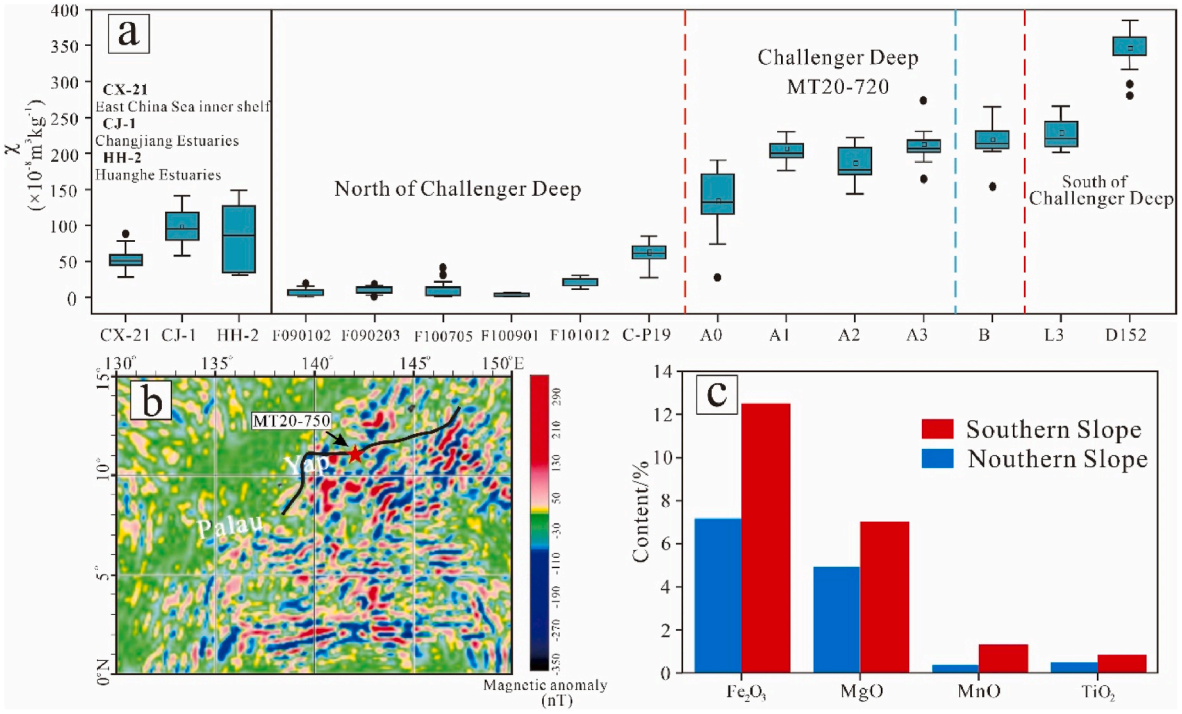

Fig. 10. (a) The χ box plots of sediment column samples from the region near the Mariana Trench (A0, A1, A2, A3 and B) (This study), East China Sea inner shelf data of sample CX-21 (Ma, 2011); Samples CJ-1 and HH-2, originating from the Changjiang-Huanghe Estuaries (Wang et al., 2004); samples of F100901-F101012 (Meng et al., 2006) (Fig. 1a), sample C-P19 (Xiao et al., 2020a) in North of Challenger Deep area; data of sample L3 (Unpublished data); sample D152 (Chen et al., 2020) in South of Challenger Deep. (b) Deep magnetic anomaly map of the study area and surrounding regions. Note: Yap Trench, Palau Ridge (Hu et al., 2014). (c) Comparison of principal elements of sediments from the south and north slopes of Challenger Deep (Xie et al., 2024).

4.4. Magnetic weakening of sediments in the Challenger Deep

4.4.1. Magnetic weakening in section A2

Overall, the magnetic properties of the sediments in the Challenger Deep are notably stronger than those in other sedimentary environments, but Sections A0 and A2 exhibit weaker magnetic properties. The sediment average magnetic susceptibility in Section A2 is 184 × 10^{-8} m^3/kg and is lower than the other sections of A1, A3 and B, whose average magnetic susceptibilities are larger than 200 × 10^{-8} m^3/kg. Meanwhile, a prominent feature of Section A2 is the abrupt increase in aluminum content (Fig. 6). Aluminum, the most abundant metal element in the Earth's crust, is frequently employed in geological studies to quantify the contribution of terrigenous input (Murray et al., 1993). Given the Mariana Trench's remote location from landmasses, the high aluminum content cannot be attributed to river input. Furthermore, there is no obvious index of aeolian dust input in Section A2, suggesting that the elevated aluminum levels are not influenced by terrigenous river or aeolian dust input.

Murray and Leinen (1996) discovered in their investigation of Al/Ti ratios in equatorial Pacific carbonate sediments that this ratios can reach up to three times the Al/Ti ratio found in Post-Archean Average Shale (PASS). They termed the additional Al as "excess aluminum" (Alxs). Further research has demonstrated a positive correlation between Alxs and biogenic materials (such as opal and carbonate) in sediments, suggesting that Alxs is associated with surface water productivity. Alxs results from the removal of dissolved Al in seawater by biogenic particles (Kryc et al., 2003; Nambiar et al., 2022). Under the scanning electron microscope, a significant amount of diatom debris was observed in the A2 layer of the core (Fig. 4cde). The proliferation of diatoms significantly reduces the content of magnetic mineral particles in this layer, leading to a notable decrease in magnetic susceptibility values in the A2 layer. Therefore, the high aluminum in Section A2 can be attributed to the enhanced productivity in surface waters leading to higher Alxs, which in turn results in the magnetic weakening of sediments due to the dilution effect of diatom proliferation on magnetic minerals.

4.4.2. Shifts in provenance and magnetic weakening in section A0

The magnetic susceptibility in Section A0 is 131 × 10^{-8} m^3/kg, which amounts to only 61% and 66% of that in Section B and Section A1, respectively. The average grain size of the sediment in Section A0 is 28.2 μm, approximately 1.5–2 times larger than that in Section B and A1. This suggests a notable shift in sediment sources within Section A0.

The aeolian dust content (EM1 end) is the lowest in Section A0, sediment source from the Pacific Plate (EM2) decrease, and sediment source from the Philippine Sea Plate (EM2) increase in Section A0. The ^{14}C data reveal an age reversal in Section A0, with an age exceeding 5000 years, which is relatively old compared to Section A1. This indicates that older sediments from the Philippine Sea Plate contribute more significantly to the sediment in the Challenger Deep in Section A0. This may be attributed to earthquakes, volcanic eruptions, or other intense geological activities. However, this process occurs gradually and continuously. As shown in Fig. 11, between 28 cm and 15 cm (approximately 13 cm in thickness), a reversal in sediment age from approximately 5100 years is observed. Simultaneously, both magnetic properties and chemical parameters exhibit a gradual decline, whereas grain size shows an increasing trend, suggesting a continuous influx of coarser sediment from the northern source into the trench bottom. Assuming a deposition rate of 1.3 mm per annual in this region, the enhanced contribution of northern sediments persisted for over ten years.

In this section, the supply of northern sources represented by EM3 is at its maximum, indicating increased material supply from the north during this period (Figs. 8 and 11). Notably, as the chronological sequence reverses, the proportion of northern materials (EM3) experiences a substantial surge from 10% to 45%, followed by a sudden decline to 3%, and subsequently a gradual ascent back to 30% (Figs. 8 and 11). Subsequently, between 15 cm and 4 cm depth, the sedimentary makeup reverts to being predominantly derived from the southern slope, with

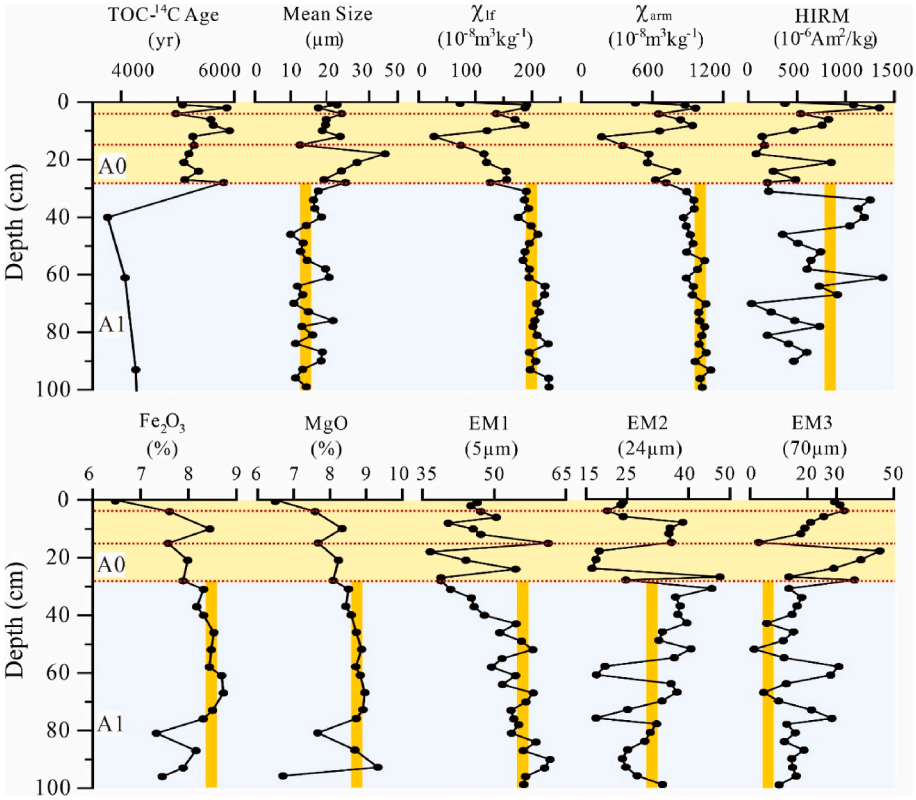

Fig. 11. Changes in magnetic susceptibility of section A0.

the northern slope's contribution tapering off. However, from 4 cm to the surface (0 cm), there is evidence of renewed sediment supply from the northern slope, indicating the dynamic interplay between sediment sources over time.

In summary, the processes occurred in Section A0 reveal significant tectonic activity marked by the rapid surge and fluctuations in northern materials (EM3). These observations suggest a prolonged tectonic event potentially involving both volcanic and seismic activities. A temporary lull in activity is succeeded by renewed, albeit less intense, tectonic movements, thereby underlining the dynamic and episodic nature of geological processes in this region.

4.5. Sedimentation patterns in the axis of the Challenger Deep

The material supply dynamics within oceanic trenches represent an active and ever-changing process, intricately influenced by a variety of factors. Among these, the material sources play a important role, encompassing aeolian dust sediments, biogenic inputs, and diverse parent rock compositions from both the northern and southern trench flanks. These sediment inputs generally maintain a dynamic equilibrium in sedimentary patterns. However, this equilibrium is notably modulated by climatic factors, including wind-driven transport and intra-trench ocean currents, as well as geological forces generated by earthquakes and volcanic eruptions. Although the Challenger Deep lacks historical seismic records in sediments, the Mariana Trench, as a typical component of an oceanic convergent plate boundary (Gribble et al., 1996; Stern et al., 2003), is known for its high seismic activity. In fact, a six-month OBS seismic observation conducted in the southern Mariana Trench in 2016 recorded over 7000 local earthquakes (Zhu et al., 2019). Therefore, seismic activity could also be a reason for the increased input of northern material.

Overall, the sedimentary regime of the trench is primarily characterized by the erosion of the surrounding rocks of the Pacific Plate, with detrital materials (around 35%) transported and deposited by the dynamic forces of Antarctic Bottom Water (AABW). The erosive capacity of AABW remains relatively stable over a millennial timescale. Concurrently, the trench receives substantial eolian dust inputs from distant sources, closely linked to climatic variations, contributing an estimated 50% of the sedimentary load. Furthermore, indirect contributions from the augmentation of biogenic materials and episodic geological perturbations, notably earthquakes and volcanic eruptions, serve to enhance the influx of materials originating from the Philippine Sea Plate, accounting for an additional 5% of the sedimentary composition.

Importantly, geological events disrupt the sedimentary equilibrium, acting as catalysts for increased transport of northern-sourced materials. Analysis of ^{14}C data from sediment cores spanning the entire core reveals multiple instances of age inversions at depth. These anomalies suggest frequent disruptions in sediment accumulation patterns, particularly during geological events like earthquakes and volcanic eruptions, confirming enhanced input of northern-sourced materials up to 30% under such dynamic conditions. Concurrently, dust input decreases to 35%, while sediment from the Pacific Plate remains around 35% (Fig. 12). Due to the limitation of data in section B, we are unable to analyze the detail magnetic properties change, however, the several age inversions of this core also give an indication that the dynamic equilibrium of sedimentary patterns is interrupted very often in the Challenger due to the frequent geological activities.

5. Conclusion

1) Parameters of magnetism, grain size and geochemistry show that the sediment sources in the Challenger Deep are generally from Asian dust input (around 35–50%), altered bedrock sediment components in the Pacific Plate (around 30–45%) and the volcanic eruption materials in the Philippine Sea Plate and biogenetic materials (around 5–35%).
2) Sediments in the Challenger Deep exhibit strong magnetic properties compared to other oceanic and trench sediments, with magnetic susceptibility 5–20 times higher than in other regions, including deep sea, shelf and estuaries.
3) The strong magnetic properties of the sediments in the Challenger Deep are due to the enhanced alteration of subducting plate rocks, primarily composed of ferromagnesian basalt, by bottom water. This process forms sediments that are funneled into the trench axis and preserved in an oxidizing environment.
4) The relative lower magnetic properties in this core show the increase input of biogenetic materials, or lower magnetic sediments from the Philippine Sea Plate caused by the earthquake or other geological activities.
5) The sedimentation pattern in the trench indicates that, under normal circumstances, the Challenger Deep mainly receives material from the Pacific Plate and dust input. Occasionally event deposits from the northern slope increase gradually caused by geological processes or biogenetic materials.

CRediT authorship contribution statement

KaiWei Wang: Writing – review & editing, Software, Methodology, Data curation. **YongHong Wang:** Writing – review & editing, Supervision, Resources, Project administration, Conceptualization. **QiuYu Yue:**

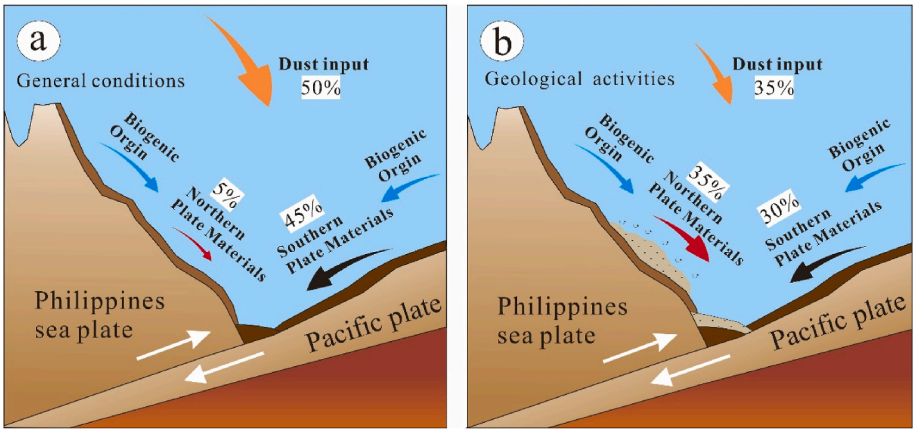

Fig. 12. Sedimentation Patterns in the MT20-750 Sediment Core from the Challenger Deep. The Pacific Plate acts as the underlying plate, while the Philippine Sea Plate is the overlying plate. (a) Sediment supply is predominantly from the Pacific Plate, as seen in Section B layer. (b) Material input from the Philippine Sea Plate increases in Section A layer, with event deposition occurring in certain sections (e.g., Section A0).

Validation, Software, Methodology, Investigation. **XiaoHua Zhang:** Validation, Formal analysis, Data curation. **JiWen Liu:** Methodology, Investigation, Data curation. **Chunhui Xiao:** Methodology, Formal analysis, Data curation. **Toshiya Kanamatsu:** Methodology, Data curation. **Michael Strasser:** Writing – review & editing. **Rui Bao:** Writing – review & editing.

Declaration of competing interest

The authors declare that they have no known competing financial interests or personal relationships that could have appeared to influence the work reported in this paper.

Acknowledgments

This research was funded jointly by the General Program of National Natural Science Foundation of China (42376163), the Special Survey of Basic Scientific and Technological Resources (2022FY202402), the Shandong Provincial Natural Science Foundation, China (ZR2022MD109), and National Key Research and Development Program (2016YFC0402602). This research also used samples and data provided by the vessel *Dongfanghong*

Data availability

Data will be made available on request.

References

Banerjee, S.K., King, J., Marvin, J., 1981. A rapid method for magnetic granulometry with applications to environmental studies. Geophys. Res. Lett. 8, 333–336. https://doi.org/10.1029/GL008i004p00333.

Bloomer, S.H., 1987. Geochemical characteristics of boninite-and tholeiite-series volcanic rocks from the Mariana forearc and the role of an incompatible element-enriched fluid in arc petrogenesis. Geol. Soc. Am., Spec. Pap. 215, 151–164. https://doi.org/10.1130/SPE215-p151.

Bloomer, S.H., 1983. Distribution and origin of igneous rocks from the landward slopes of the Mariana Trench: Implications for its structure and evolution. J. Geophys. Res. Solid Earth 88, 7411–7428. https://doi.org/10.1029/JB088iB09p07411.

Bongiovanni, C., Stewart, H.A., Jamieson, A.J., 2022. High-resolution multibeam sonar bathymetry of the deepest place in each ocean. Geosci. Data J. 9, 108–123. https://doi.org/10.1002/gdj3.122.

Chen, Y., Yang, J., Dada, O.A., Yang, Y., Lin, Z., Cui, Z., Xu, Y., Yu, H., Liu, B., 2020. Magnetic properties indicate the sources of hadal sediments in the Yap Trench, northwest Pacific Ocean. J. Oceanol. Limnol. 38, 665–678. https://doi.org/10.1007/s00343-019-8370-z.

Deng, X.G., Liang, Yi, Yi, L., Paterson, G.A., Qin, H.F., Wang, H.F., Yao, H.Q., Ren, J.B., Ge, J.Y., Xu, H.Z., Deng, C.L., Zhu, R.X., 2016. Magnetostratigraphic evidence for deep-sea erosion on the Pacific Plate, south of Mariana Trench, since the middle Pleistocene: potential constraints for Antarctic bottom water circulation. Int. Geol. Rev. 58, 49–57. https://doi.org/10.1080/00206814.2015.1055597.

Evans, M., Heller, F., 2003. Environmental Magnetism: Principles and Applications of Enviromagnetics. Elsevier. Academic Press.

Gao, L.J., Zhang, J., Wu, S.G., 2017. Analysis of lithospheric rheological structure and dynamics of the Challenger Deep in Mariana trench. J. Univ. Chin. Acad. Sci. 34, 380–388. https://doi.org/10.7523/j.issn.2095-6134.2017.03.012.

Gribble, R.F., Stern, R.J., Bloomer, S.H., Stüben, D., O'Hearn, T., Newman, S., 1996. MORB mantle and subduction components interact to generate basalts in the southern Mariana Trough back-arc basin. Geochim. Cosmochim. Acta. 60, 2153–2166. https://doi.org/10.1016/0016-7037(96)00078-6.

Hu, Z.W., Chen, C., Wang, Q.G., Du, J.S., Zhang, S.X., Wang, L.S., Wang, H.R., Li, R., 2014. Characteristies of magnetic anomalies in the Philippine Sea Plate lithosphere. Earth Science 39 (11), 1735–1743. https://doi.org/10.3799/dqkx.2014.157 (In Chinese with an abstract in English).

Jamieson, A., 2015. The Hadal Zone: Life in the Deepest Oceans. Cambridge University Press.

Jiang, Z.Z., Sun, Z.L., Liu, Z.Q., Cao, H., Geng, W., Xu, H.X., Wang, L.S., 2019. Rare-earth element geochemistry reveals the provenance of sediments on the southwestern margin of the Challenger Deep. J. Oceanol. Limnol. 37, 998–1009. https://doi.org/10.1007/s00343-019-8046-8.

Kashiwabara, T., Toda, R., Nakamura, K., Yasukawa, K., Fujinaga, K., Kubo, S., Nozaki, T., Takahashi, Y., Suzuki, K., Kato, Y., 2018. Synchrotron X-ray spectroscopic perspective on the formation mechanism of REY-rich muds in the Pacific Ocean. Geochim. Cosmochim. Acta. 240, 274–292. https://doi.org/10.1016/j.gca.2018.08.013.

Kato, Y., Fujinaga, K., Nakamura, K., Takaya, Y., Kitamura, K., Ohta, J., Toda, R., Nakashima, T., Iwamori, H., 2011. Deep-sea mud in the Pacific Ocean as a potential resource for rare-earth elements. Nat. Geosci. 4, 535–539. https://doi.org/10.1038/ngeo1185.

King, J., Banerjee, S.K., Marvin, J., Özdemir, Ö., 1982. A comparison of different magnetic methods for determining the relative grain size of magnetite in natural materials: some results from lake sediments. Earth Planet Sci. Lett. 59, 404–419. https://doi.org/10.1016/0012-821X(82)90142-X.

King, J.W., Channell, J.E.T., 1991. Sedimentary magnetism, environmental magnetism, and magnetostratigraphy. Rev. Geophys. 29, 358–370. https://doi.org/10.1002/rog.1991.29.s1.358.

Kryc, K.A., Murray, R.W., Murray, D.W., 2003. Al-to-oxide and Ti-to-organic linkages in biogenic sediment: relationships to paleo-export production and bulk Al/Ti. Earth Planet Sci. Lett. 211, 125–141. https://doi.org/10.1016/S0012-821X(03)00136-5.

Larson, E.E., Reynolds, R.L., Ozima, M., Aoki, Y., Kinoshita, H., Zasshu, S., Kawai, N., Nakajima, T., Hirooka, K., Merrill, R., Levi, S., 1975. Paleomagnetism of miocene volcanic rocks of Guam and the curvature of the southern mariana Island Arc: Japan–united ststes paleomagnetism Project in Micronesia. Geol. Soc. Am. Bull. 86, 346–350. https://doi.org/10.1130/0016-7606(1975)86<346:POMVRO>2.0.CO;2.

Liu, J.W., Li, D.W., He, X.X., Liu, R.H., Cheng, H.J., Su, C.L., Chen, M.N., Wang, Y.H., Zhao, Z.S., Xu, H.Y., Cheng, Z.Y., Wang, Z.C., Pedentchouk, N., Lea-Smith, D.J., Todd, J.D., Liu, X.S., Zhang, X.H., 2024. A unique subseafloor microbiosphere in the Mariana Trench driven by episodic sedimentation. Mar. Life Sci. Technol. 6 (1), 168–181. https://doi.org/10.1007/s42995-023-00212-y.

Liu, Q.S., Roberts, A.P., Larrasoaña, J.C., Banerjee, S.K., Guyodo, Y., Tauxe, L., Oldfield, F., 2012. Environmental magnetism: principles and applications. Rev. Geophys. 50 (4), RG4002. https://doi.org/10.1029/2012RG000393.

Luo, M., Algeo, T.J., Tong, H.P., Gieskes, J., Chen, L.Y., Shi, X.F., Chen, D.F., 2018. More reducing bottom-water redox conditions during the Last Glacial Maximum in the southern Challenger Deep (Mariana Trench, western Pacific) driven by enhanced productivity. Deep Sea Res., Part II. 155, 70–82. https://doi.org/10.1016/j.dsr2.2017.01.006.

Luo, M., Gieskes, J., Chen, L.Y., Shi, X.F., Chen, D.F., 2017. Provenances, distribution, and accumulation of organic matter in the southern Mariana Trench rim and slope: implication for carbon cycle and burial in hadal trenches. Mar. Geol. 386, 98–106. https://doi.org/10.1016/j.margeo.2017.02.012.

Maher, B.A., 1988. Magnetic properties of some synthetic sub-micron magnetites. Geophys. J. Int. 94, 83–96. https://doi.org/10.1111/j.1365-246X.1988.tb03429.x.

McManus, J., 1988. Grain size determination and interpretation. Techniques in Sedimentology. Blackwell Scientific Public, Oxford, pp. 63–85.

Meng, Q.Y., Li, A.C., Jin, N., Xu, Z.K., Liu, J.G., 2006. Magnetostratigraphic and magnetic properties of marine sediments from the East Philippine sea. Mar. Geol. Quat. Geol. 3, 57–63. https://doi.org/10.16562/j.cnki.0256-1492.2006.03.009 (In Chinese with an abstract in English).

Meng, Q.Y., Li, A.C., Jiang, F.Q., Xu, Z.K., Liu, J.G., 2007. Relative intensity record of geomagnetic field in sediments from the eastern Philippine Sea. In: Proceedings of the 23rd Annual Meeting of the Chinese Geophysical Society. Institute of Oceanology. Chinese Academy of Sciences, Qingdao, China, p. 471.

Migdisov, A.A., Miklishansky, A.Z., Saveliev, B.V., Bredanova, N.V., Girin, Y.P., 1981. 28. Neutron activation analysis of rare earth elements and some other trace elements in volcanic ashes and pelagic clays. deep sea drilling project leg 59, 653–668. https://doi.org/10.2973/DSDP.PROC.59.128.1981.

Murray, R.W., Leinen, M., 1996. Scavenged excess aluminum and its relationship to bulk titanium in biogenic sediment from the central equatorial Pacific Ocean. Geochim. Cosmochim. Acta. 60, 3869–3878. https://doi.org/10.1016/0016-7037(96)00236-0.

Murray, R.W., Leinen, M., Isern, A.R., 1993. Biogenic flux of Al to sediment in the central equatorial Pacific Ocean: evidence for increased productivity during glacial periods. Paleoceanography 8, 651–670. https://doi.org/10.1029/93PA02195.

Ma, H.L., 2011. Magnetic properties of core sediments off the Yangtze River Estuary and East China Sea inner shelf and their influencing factors. East China Normal University, pp. 1–84. Master thesis.

Nambiar, R., Bhushan, R., Raj, H., 2022. Paleoredox conditions of bottom water in the northern Indian Ocean since 39 ka. Palaeogeogr. Palaeoclimatol. Palaeoecol. 586, 110766. https://doi.org/10.1016/j.palaeo.2021.110766.

Paterson, G.A., Heslop, D., 2015. New methods for unmixing sediment grain size data. Geochem., Geophys., Geosyst. 16, 4494–4506. https://doi.org/10.1002/2015GC006070.

Peters, C., Dekkers, M.J., 2003. Selected room temperature magnetic parameters as a function of mineralogy, concentration and grain size. Phys. Chem. Eart A/B/C. 28, 659–667. https://doi.org/10.1016/S1474-7065(03)00120-7.

Reagan, M.K., McClelland, W.C., Girard, G., Goff, K.R., Peate, D.W., Ohara, Y., Stern, R. J., 2013. The geology of the southern Mariana fore-arc crust: implications for the scale of Eocene volcanism in the western Pacific. Earth Planet Sci. Lett. 380, 41–51. https://doi.org/10.1016/j.epsl.2013.08.013.

Roberts, A.P., 1995. Magnetic properties of sedimentary greigite (Fe_3S_4). Earth Planet Sci. Lett. 134, 227–236. https://doi.org/10.1016/0012-821X(95)00131-U.

Shao, Y.P., Wyrwoll, K.-H., Chappell, A., Huang, J.P., Lin, Z.H., Mctainsh, G.H., Mikami, M., Tanaka, T.Y., Wang, X.L., Yoon, S., 2011. Dust cycle: an emerging core theme in Earth system science. Aeolian Res 2 (4), 181–204. https://doi.org/10.1016/j.aeolia.2011.02.001.

Shepard, F.P., 1954. Nomenclature based on sand-silt-clay ratios. J. Sediment. Res. 24, 151–158. https://doi.org/10.1306/D4269774-2B26-11D7-8648000102C1865D.

Song, Z.J., Meng, F.Y., Li, W.D., Chen, L.Y., Luo, M., 2022. Preliminary study on source and sedimentary environment in the Mariana Trench. Mar. Geol. Quat. Geol. 42 (4), 84–100. https://doi.org/10.16562/j.cnki.0256-1492.2022031801 (In Chinese with an abstract in English).

Stern, R.J., Fouch, M.J., Klemperer, S.L., 2003. An overview of the Izu-Bonin-Mariana subduction factory. Geophysical Monograph-American Geophysical Union 138, 175–222. https://doi.org/10.1029/138GM10.

Strasser, M., Ikehara, K., Pizera, C., Itaki, T., Satoguchi, Y., Proust, J.N., Sawyer, D., , IODP Expedition 386, Kioka, A., McHugh, C., Expedition Management Team, IODP Expedition 386 Expedition Science Party, 2024. Japan Trench event stratigraphy: first results from IODP giant piston coring in a deep-sea trench to advance subduction zone paleoseismology. Mar. Geol. 477, 107387. https://doi.org/10.1016/j.margeo.2024.107387.

Su, C.J., Xu, Z.L., Zhang, D.L., Liu, Q., Liu, J.Z., 2023. Aeolian dust history since 14. 4 cal. ka B. P. indicated by grain-size end members of Shayan loess in the southern Kazakhstan. Quat. Sci. 43, 46–56. https://doi.org/10.11928/j.issn.1001-7410.2023.01.04 (In Chinese with an abstract in English).

Taira, K., Kitagawa, S., Yamashiro, T., Yanagimoto, D., 2004. Deep and bottom currents in the Challenger Deep, Mariana Trench, measured with super-deep current meters. J. Oceanogr. 60, 919–926. https://doi.org/10.1007/s10872-005-0001-y.

Thompson, R., Oldfield, F., 1986. Environmental magnetism. Allen and Unwin, London, pp. 1–227.

Tian, L.Y., Zhao, G.T., Chen, Z.L., Wang, Y.L., Wu, S.Y., 2003. The preliminary study of petrological geochemistry of basalts from hydrothermal activity regions, Mariana Trough. J. Ocean Univ. Qingdao 3, 405–412. https://doi.org/10.16441/j.cnki.hdxb.2003.03.012 (In Chinese with an abstract in English).

Turnewitsch, R., Falahat, S., Stehlikova, J., Oguri, K., Glud, R.N., Middelboe, M., Kitazato, H., Wenzhöfer, F., Ando, K., Fujio, S., Yanagimoto, D., 2014. Recent sediment dynamics in hadal trenches: evidence for the influence of higher-frequency (tidal, near-inertial) fluid dynamics. Deep-Sea Res., Part A I. 90, 125–138. https://doi.org/10.1016/j.dsr.2014.05.005.

Tang, H.N., 2021. Distribution Patterns of Environmental Magnetism in Atlantic Sediments and Analysis of Their Source Sink Indicators. Ocean University of China, Ms Thesis.

Wang, C., 2020. Geochemical characteristics and geological significance of the sediments of western Philippines basin (western pacific). China University of Petroleum. https://doi.org/10.27644/d.cnki.gsydu.2020.000969.

Wang, F.L., He, G.W., Wang, H.F., Ren, J.B., 2016. Geochemistry of rare earth elements in a core from mariana trench and its significance. Mar. Geol. Quat. Geol. 36, 67–75. https://doi.org/10.16562/j.cnki.0256-1492.2016.04.008.

Wang, S.Q., Wei, D.L., Zhang, W., 2022. The End-member characteristics of the grain size of the aeolian sand deposits in the Liaodong Peninsula since the last glacial period and the study on paleoclimate evolution. Quat. Sci. 42, 338–349. https://doi.org/10.11928/j.issn.1001-7410.2022.02.02 (In Chinese with an abstract in English).

Wang, Y.H., Shen, H.T., Zhang, W.G., 2004. A preliminary comparison of magnetic properties of sediments from the Changjiang and the huanghe estuaries. Acta Sedimentol. Sin. 4, 658–663. https://doi.org/10.14027/j.cnki.cjxb.2004.04.016 (In Chinese with an English abstract).

Wang, Y.H., Wang, S., Liu, M., 2017. Magnetic properties indicate sediment provenance and distribution patterns in the Bohai and Yellow Seas, China. Cont. Shelf Res. 140, 84–95. https://doi.org/10.1016/j.csr.2017.04.012.

Wen, Q.Z., Diao, G.Y., Pan, J.Y., Wu, M.Q., 1996. Comparison of average chemical composition of loess in loess plateau with clark values of crust. Acta Pedol. Sin. 3, 225–231.

Wood, D.A., Mattey, D.P., Joron, J.L., Marsh, N.G., Treuil, M., 1981. A Geochemical Study of 17 Selected Samples from Basement Cores Recovered at Site 447, 448, 449, 450 and 451, Deep Sea Drilling Project Leg 59. Init. Rep. Deep Sea Drill, vol. 59. Proj., pp. 743–752

Xiao, C.H., Wang, Y.H., Lin, J., 2020a. Constraints of magnetostratigraphic and mineralogical data on the provenance of sediments in the Parece Vela Basin of the western Pacific. J. Asian Earth Sci. 196, 104373. https://doi.org/10.1016/j.jseaes.2020.104373.

Xiao, C.H., Wang, Y.H., Tian, J.W., Wang, X.C., Xin, Y., 2020b. Mineral composition and geochemical characteristics of sinking particles in the Challenger Deep, Mariana Trench: implications for provenance and sedimentary environment. Deep-Sea Res., Part A I. 157, 103211. https://doi.org/10.1016/j.dsr.2019.103211.

Xiao, C.H., Wang, Y.H., Lin, J., Tian, J.W., 2021. Characteristics of rare earth elements in deep-water sediments in Mariana "Trench-Basin" system and their provenance constraints. Mar. Geol. Quat. Geol. 41 (1), 102–114. https://doi.org/10.16562/j.cnki.0256-1492.2020040202 (In Chinese with an abstract in English).

Xie, Y.X., Yang, X.Q., Zhang, H.D., Chen, Q., Li, G.H., 2019. Eolian input and East Asian winter monsoon records in deep-sea sediment from Western Pacific since -80 ka. J. Palaeogeogr. 21 (5), 855–868. https://doi.org/10.7605/gdkb.2019.05.058 (In Chinese with an abstract in English).

Xie, T.T., Peng, X.T., Liu, S.Q., Xu, H.C., Xu, W.J., 2024. Geochemical characteristics and formation mechanism of sediments from the challenger deep in the southern Mariana Trench. Acta Sedimentol. Sin. 42 (3), 944–955. https://doi.org/10.14027/j.issn.1000-0550.2022.104 (In Chinese with an abstract in English).

Xu, Z.K., Li, A.C., Jiang, F.Q., Xu, F.J., 2008. Geochemical character and material source of sediments in the eastern Philippine Sea. Chin. Sci. Bull. 53, 923–931. https://doi.org/10.1007/s11434-008-0118-7.

Xu, Z.K., Li, T.G., Clift, P.D., Lim, D., Wang, S.M., Chen, H.J., Tang, Z., Jiang, F.Q., Xiong, Z.F., 2015. Quantitative estimates of Asian dust input to the western Philippine Sea in the mid-late Quaternary and its potential significance for paleoenvironment. Geochem., Geophys., Geosyst. 16 (9), 3182–3196. https://doi.org/10.1002/2015GC005929.

Yamazaki, T., 2009. Environmental magnetism of pleistocene sediments in the north pacific and ontong-java plateau: temporal variations of detrital and biogenic components. Geochem., Geophys., Geosyst. 10 (7), 1–18. https://doi.org/10.1029/2009GC002413.

Zhang, F., Lin, J., Zhan, W.H., 2014. Variations in oceanic plate bending along the Mariana trench. Earth Planet Sci. Lett. 401, 206–214. https://doi.org/10.1016/j.epsl.2014.05.032.

Zhang, L.L., Hu, B.Q., Qiu, Z.Y., Guo, J.W., Ding, X., Lu, J., Xiang, R., 2021. Records of polycystine radiolaria in the diatom mats sediments from the western Philippine Sea and their environmental significance. Earth Sci. 46, 853–865. https://doi.org/10.3799/dqkx.2020.341 (In Chinese with an abstract in English).

Zhou, Y., Jiang, F.Q., Xu, Z.K., Fang, H.C., Zhang, J., Li, A.C., 2015. Grain-size distribution of detrital sediment in the Parece Vela Basin and its implication of provenance and palaeoclimate over the last 2 Ma. Mar. Sci. 39, 86–93. https://doi.org/10.11759/hykx20140314001 (In Chinese with an abstract in English).

Zhu, G.H., Yang, H.F., Lin, J., Zhou, Z.Y., Xu, M., Sun, J.L., Wan, K.Y., 2019. Along-strike variation in slab geometry at the southern Mariana subduction zone revealed by seismicity through ocean bottom seismic experiments. Geophys. J. Int. 218, 2122–2135. https://doi.org/10.1093/gji/ggz272.